Structural Engineering and Mechanics, *Vol. 59, No. 2 (2016) 243-259*
DOI: http://dx.doi.org/10.12989/sem.2016.59.2.243

Transient response analysis of tapered FRP poles with flexible joints by an efficient one-dimensional FE model

Behnam Saboori*[1] and Seyed Mohammad Reza Khalili[2,3a]

[1]*Center of Excellence in Experimental Solid Mechanics and Dynamics, School of Mechanical Engineering, Iran University of Science and Technology, Narmak, Tehran 16846, Iran*
[2]*Center of Excellence for Research in Advanced Materials & Structures, Faculty of Mechanical Engineering, K.N. Toosi University of Technology, Tehran, Iran*
[3]*Faculty of Engineering, Kingston University, UK*

(Received July 10, 2015, Revised January 6, 2016, Accepted May 3, 2016)

Abstract. This research develops a finite element code for the transient dynamic analysis of tapered fiber reinforced polymer (FRP) poles with hollow circular cross-section and flexible joints used in power transmission lines. The FRP poles are modeled by tapered beam elements and their flexible joints by a rotational spring. To solve the time equations of transient dynamic analysis, precise time integration method is utilized. In order to verify the utilized formulations, a typical jointed FRP pole under step, triangular and sine pulses is analyzed by the developed finite element code and also ANSYS commercial finite element software for comparison. Thereafter, the effect of joint flexibility on its dynamic behavior is investigated. It is observed that by increasing the joint stiffness, the amplitude of the pole tip deflection history decreases, and the time of occurrence of the maximum deflection is earlier.

Keywords: transmission pole; fiber-reinforced; transient dynamic; finite element (FE); flexible joint

1. Introduction

The unique characteristics of fiber reinforced polymers (FRP) such as their high strength-to-weight ratio, resistance to corrosion, high energy absorption, and the lower transportation, installation and maintenance costs due to their light weight, made them suitable to use for manufacturing power transmission poles as a replacement of conventional materials (wood, concrete and steel). FRP transmission poles are made of polymer matrix with reinforcing fibers, mostly fabricated by filament winding technique. Polyester, vinylester or epoxy is mainly used as matrix and E-glass, S-glass, aramid or carbon fibers as reinforcement (Ibrahim *et al*. 2000).

In contrast with conventional steel/wood transmission poles, there are little advanced design and analysis approaches focused on the FRP poles (Metiche and Masmoudi 2012, Metiche *et al*. 2009). In general, transmission poles are mainly subjected to dynamic cantilever bending due to wind gusts and cable unilateral failure, or may also be subjected to vehicle impacts. The poles are

*Corresponding author, Ph.D. Candidate, E-mail: b_saboori@iust.ac.ir
[a]Professor, E-mail: smrkhalili2005@gmail.com

http://www.techno-press.org/?journal=sem&subpage=8 ISSN: 1225-4568 (Print), 1598-6217 (Online)

mostly tapered and thin-walled members. Many studies are performed on the dynamic behavior of thin-walled sections made of steel as well as composite materials, but only a few are on tapered sections. In fact, the previous studies are concerned with the dynamic behavior of tapered members made from homogeneous and isotropic materials (Polyzois *et al*. 1998). Because of the complexity of material properties, layer lay-ups, fiber orientations, tapered shape, and combination of loads of FRP transmission poles, the pure analytical method is incapable of providing acceptable solutions effectively, but the numerical analysis methods (specially the finite element method) are proved to be more efficient (Lin 1995). Navaratna *et al*. (1968) are among the early researchers to use the finite element method (FEM) to analyze the stability of the shells of revolution. The approach used by them to develop the geometric stiffness matrix is followed by Gould and Basu (1977) for the linear buckling and the incremental deformation analysis of rotational shells. Zabihollah and Ganesan (2010) conducted the buckling analysis of laminated tapered composite beams using a higher order finite element formulation that ensures the continuity of the stress distribution through the thickness of a laminate as well as across the element interfaces. There are also other researches dealing with the static and stability analysis of the thin-walled FRP poles by FEM (Fam *et al*. 2010, Polyzois and Raftoyiannis 2009, Saboori and Khalili 2011).

Both the analytical methods and FE techniques have also been employed for the transient response analysis of various engineering problems (for example see (Bae *et al*. 2016, Han *et al*. 2016)). Mabie and Rogers (1972, 1974) presented a closed-form solution to the free vibration of an isotropic double-tapered cantilever beam with rectangular cross-section and end mass. The beam was tapered linearly in the horizontal and vertical planes simultaneously, with the taper ratio in the horizontal plane equal to that in the vertical plane. Noor *et al*. (1991) assessed a group of computational methods for multilayered composite cylinders. The finite element models they surveyed are mostly two or three-dimensional elements. Khdeir *et al*. (1989) studied the vibration and buckling of cross-ply circular cylindrical shells with various shell theories. The different approaches of inclusion of transverse shear strains were discussed. Caracoglia and Jones (2007) performed a numerical and experimental study of vibration mitigation for highway tapered aluminum poles. The study was performed in order to identify the potential causes associated with the failures. It was concluded that, although the poles were designed according to standard specifications, an unusual event, in which the combination of wind and frozen precipitation was observed, could be responsible for large vibration amplitudes. Xiang *et al*. (2011) analyzed the free vibration characteristics of laminated composite cylindrical and spherical shells by the first-order shear deformation theory and a meshless global collocation method based on thin plate spline radial basis function. Polyzois *et al*. (1998) investigated the free vibration of tapered GFRP poles using tapered beam element. In their work, the natural frequency and period of the fundamental flexural vibration mode of the pole were computed for various cases of lamination angle, taper ratio, and mass at the top. Raftoyiannis and Polyzois (2007) surveyed the effect of semi-rigid connections on the free vibration of tapered GFRP poles by FEM. In their work, modal analysis was performed for design purposes to obtain the natural frequency and period of poles with various geometrical characteristics and material lay-up, as well as the effect of connection flexibility. Experimental results on the free vibration behavior of jointed composite poles were also presented. Finite element method was used by Ibrahim and Polyzois (1999) to analyze the cross-section ovalization behavior of FRP poles under a bending load. Based on their study, circumferential layers tend to increase the critical ovalization load of FRP poles. In the work of Caracoglia (2007), two problems are analyzed: the susceptibility to across-wind galloping-type

vibration associated with the deposit of frozen-precipitation on the surface of the poles or the luminaire, installed at the top of the unit; and the influence of eccentric aerodynamic loading at the level of the luminaire on the dry-unit buffeting response. Caracoglia and Velazquez (2008) also compared the dynamic performance of steel, aluminum and GFRP light poles through experimental testing. The comparison of the performances was based on frequency and damping ratios corresponding to the first and the second-mode vibrations.

The transient dynamic analysis of monolithic tapered FRP poles was investigated using FEM in an earlier research conducted by the authors (Khalili and Saboori 2010). Since for ease of manufacturing, transportation and erection, long transmission poles are produced modular, this paper explores the transient dynamic behavior of those FRP poles having flexible joints. In the current study, to analyze the dynamic response of tapered FRP poles, tapered beam finite element model is employed. It is assumed that the material behavior is linear elastic and the laminate of the cross-section of the wall is symmetric or anti-symmetric angle-ply. Components of the laminate stiffness matrices and the equivalent moduli used in the analysis are derived from the classical lamination theory. In order to model flexible joints of the jointed transmission poles, a simple model considering the joint as a rotational spring is utilized. The time equations of transient dynamic analysis are solved using precise time integration method. Then, a typical FRP pole with an adhesive joint is analyzed by the finite element (FE) code developed based on the mentioned formulation and also ANSYS finite element software. Once the results obtained from the provided FE code for the typical jointed pole under various pulses (step, triangular and sine pulses) were verified through the comparison with ANSYS results, the effect of joint stiffness on the dynamic behavior of the tapered FRP poles with flexible joints is investigated.

2. Effective longitudinal modulus

Using the classical lamination theory, the stiffness components of each generally orthotropic lamina can be determined and the constitutive equation for the laminate is (Jones 1999)

$$\begin{Bmatrix} N \\ M \end{Bmatrix} = \begin{bmatrix} A & B \\ B & D \end{bmatrix} \begin{Bmatrix} \varepsilon \\ \kappa \end{Bmatrix} \tag{1}$$

where $\{N\}$ and $\{M\}$ are the force and couple moment resultants, respectively. $\{\varepsilon\}$ and $\{\kappa\}$ are the strains of the mid plane and the laminated plate curvatures. The stiffness coefficients A_{ij}, B_{ij}, and D_{ij} correspond to extensional, coupling, and bending stiffness coefficients and are defined as follows (Jones 1999)

$$A_{ij} = \int_{-h/2}^{h/2} \overline{Q}_{ij} dz \tag{2}$$

$$B_{ij} = \int_{-h/2}^{h/2} z\overline{Q}_{ij} dz \tag{3}$$

$$D_{ij} = \int_{-h/2}^{h/2} z^2 \overline{Q}_{ij} dz \tag{4}$$

where h is the laminate thickness and $\overline{Q}_{ij}$ are the transformed layer stiffness components. Inverting Eq. (1) results in the following

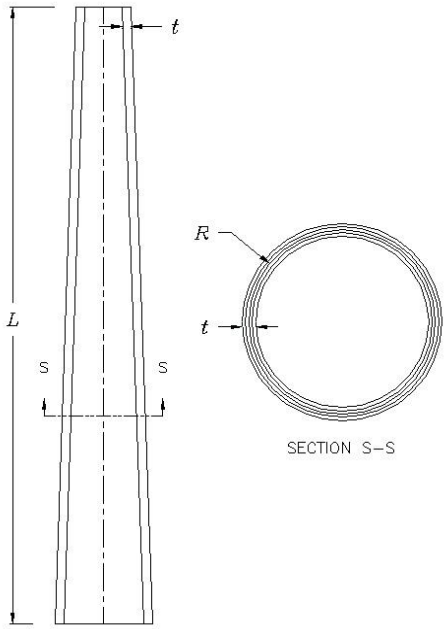

Fig. 1 General geometry of a tapered composite pole

$$\begin{Bmatrix} \varepsilon_x \\ \varepsilon_y \\ \gamma_{xy} \\ \kappa_x \\ \kappa_y \\ \kappa_{xy} \end{Bmatrix} = \begin{bmatrix} a_{11} & a_{12} & a_{16} & b_{11} & b_{12} & b_{16} \\ a_{21} & a_{22} & a_{26} & b_{21} & b_{22} & b_{26} \\ a_{61} & a_{62} & a_{66} & b_{61} & b_{62} & b_{66} \\ b_{11} & b_{21} & b_{61} & d_{11} & d_{12} & d_{16} \\ b_{12} & b_{22} & b_{62} & d_{21} & d_{22} & d_{26} \\ b_{16} & b_{26} & b_{66} & d_{61} & d_{62} & d_{66} \end{bmatrix} \begin{Bmatrix} N_x \\ N_y \\ N_{xy} \\ M_x \\ M_y \\ M_{xy} \end{Bmatrix} \tag{5}$$

The effective longitudinal elasticity modulus E_{eff} can be calculated from Eq. (5) as

$$E_{eff} = \frac{1}{a_{11}h} \tag{6}$$

In some references (Polyzois *et al*. 1998, Raftoyiannis and Polyzois 2007), an approximate equation has been used for the effective modulus E_{eff}, but Eq. (6) is the precise expression of the effective longitudinal modulus.

3. Tapered beam element

The general geometry of a tapered composite pole is shown in Fig. l. In order to approximate the dynamic behavior of the tapered poles accurately, a tapered beam finite element has been developed (Polyzois *et al*. 1998). The tapered beam element of length L and circular hollow cross-

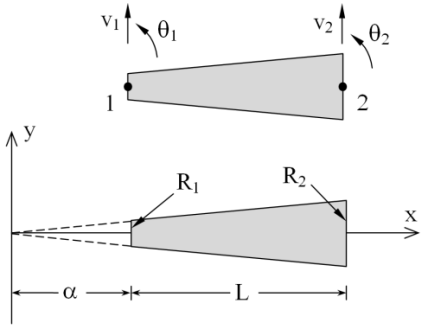

Fig. 2 Coordinate system and degrees of freedom of the tapered element

section with uniform thickness h is shown in Fig. 2. The radii at the small and the large ends are R_1 and R_2, respectively. Since the cross-section is thin-walled, the cross-sectional area and the moment of inertia are computed by $A=2\pi Rh$ and $I=\pi R^3 h$, where the radius R varies linearly over the length. This implies a linear variation of the area A and a cubic variation of the moment of inertia I with respect to the length L. Thus, it is convenient to adopt a coordinate system x-y as shown in Fig. 2, in which the area and the moment of inertia are expressed as follows

$$A = A_0 x, \; I = I_0 x \tag{7}$$

where A_0 and I_0 are coefficients defined as follows

$$A_0 = 2\pi\left(\frac{R_1}{\alpha}\right)h, \; I_0 = \pi\left(\frac{R_1}{\alpha}\right)^3 h \tag{8}$$

The shift α with respect to the coordinate origin is defined geometrically by

$$\alpha = \frac{L}{R_2/R_1 - 1} \tag{9}$$

By finite element formulating the tapered beam element in flexural vibration, its stiffness and mass matrices, $[K_f]$ and $[M_f]$, are derived as (Polyzois *et al*. 1998)

$$[K_f] = [B_f]^T [k_f][B_f] \tag{10}$$

$$[M_f] = [B_f]^T [m_f][B_f] \tag{11}$$

where

$$[B_f] = \begin{bmatrix} \alpha & \ln\alpha & \frac{1}{\alpha} & 1 \\ 1 & \frac{1}{\alpha} & -\frac{1}{\alpha^2} & 0 \\ \alpha+L & \ln(\alpha+L) & \frac{1}{\alpha+L} & 1 \\ 1 & \frac{1}{\alpha+L} & -\frac{1}{(\alpha+L)^2} & 0 \end{bmatrix}^{-1} \tag{12}$$

$$[k_f] = EI_0 \begin{bmatrix} 0 & 0 & 0 & 0 \\ 0 & \ln(\alpha+L)-\ln\alpha & \dfrac{2}{\alpha+L}-\dfrac{2}{\alpha} & 0 \\ 0 & \dfrac{2}{\alpha+L}-\dfrac{2}{\alpha} & \dfrac{2}{\alpha^2}-\dfrac{2}{(\alpha+L)^2} & 0 \\ 0 & 0 & 0 & 0 \end{bmatrix} \tag{13}$$

and the terms of $[m_f]$ are as follows

$$m_{f,11} = \frac{1}{4}\rho A_0 \left\{(\alpha+L)^4 - \alpha^4\right\} \tag{14a}$$

$$m_{f,12} = \frac{1}{9}\rho A_0 \left\{(\alpha+L)^3(3\ln(\alpha+L)-1) - \alpha^3(3\ln\alpha-1)\right\} \tag{14b}$$

$$m_{f,13} = \frac{1}{2}\rho A_0 \left\{(\alpha+L)^2 - \alpha^2\right\} \tag{14c}$$

$$m_{f,14} = \frac{1}{3}\rho A_0 \left\{(\alpha+L)^3 - \alpha^3\right\} \tag{14d}$$

$$m_{f,22} = \frac{1}{4}\rho A_0 \{(\alpha+L)^2(2\ln^2(\alpha+L) - 2\ln(\alpha+L)+1) - \alpha^2(2\ln^2\alpha - 2\ln\alpha+1)\} \tag{14e}$$

$$m_{f,23} = \rho A_0 \{(\alpha+L)(\ln(\alpha+L)-1) - \alpha(\ln\alpha-1)\} \tag{14f}$$

$$m_{f,24} = \frac{1}{4}\rho A_0 \{(\alpha+L)^2(2\ln(\alpha+L)-1) - \alpha^2(2\ln\alpha-1)\} \tag{14g}$$

$$m_{f,33} = \rho A_0 \{\ln(\alpha+L) - \ln\alpha\} \tag{14h}$$

$$m_{f,34} = \rho A_0 L \tag{14i}$$

$$m_{f,44} = \frac{1}{2}\rho A_0 \left\{(\alpha+L)^2 - \alpha^2\right\} \tag{14j}$$

and ρ is the mass density of the composite material and E is the effective longitudinal modulus.

Thus, the equilibrium equation for the tapered beam element in flexural mode (neglecting the effect of damping) can be written in the matrix form as follows

$$[M_f]\underline{\ddot{\delta}} + [K_f]\underline{\delta} = \underline{Q} \tag{15}$$

where $\underline{\delta}$ is the nodal displacement vector and $\underline{Q}$ is the nodal force vector.

In the case of symmetric laminate, all the B_{ij} terms, and in the case of anti-symmetric angle-ply laminate, all the B_{ij} terms except B_{16} and B_{26} are equal to zero. Hence, for these two types of

laminates, bending-extension coupling vanishes (it is an approximate assumption for anti-symmetric angle-ply laminate) and the axial vibration is uncoupled from the flexural vibration. Since the flexural vibration of the transmission poles is more important, in the present numerical investigation of the transient dynamic analysis, for the symmetric or anti-symmetric angle-ply laminates, the flexural mode is only evaluated. Thus, the nodal displacement vector of the tapered element in the flexural mode is

$$\underline{\delta} = \begin{Bmatrix} v_1 \\ \theta_1 \\ v_2 \\ \theta_2 \end{Bmatrix} \tag{16}$$

4. Flexible connection model

In order to ease in manufacturing, transportation and installation, long transmission poles are produced modular and then are connected together. The joint type among the parts of the long poles can be adhesive, or by screw or a combination of mechanical and adhesive bonds. In the current research work, a joint technique developed at the University of Manitoba of Canada (Raftoyiannis and Polyzois 2007) has been considered which is constructed by connecting two tapered cylindrical parts, utilizing an overlapping part of the jointed elements with length *l*, as shown in Fig. 3.

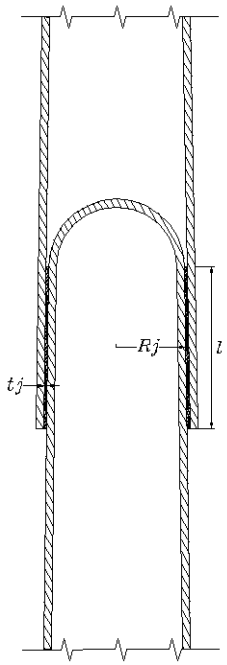

Fig. 3 The joint geometry

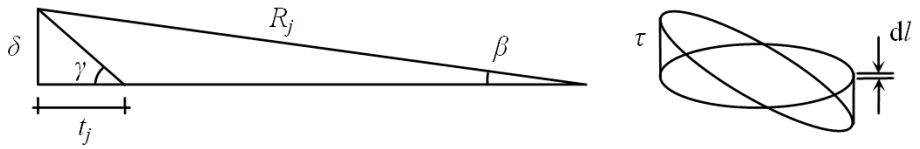

Fig. 4 Joint kinematics and shear stress distribution due to bending

A thin film with the thickness of t_j of resin (West System Epoxy 105 with hardener 206, in the mentioned case) is applied to the interface which after curing, acts as an adhesive to hold the two parts together. All member forces are transferred through the joint in the form of shear stresses τ, acting on the joint surfaces. In order to model the bending stiffness of the joint, a relation between shear strains γ of the interface resin and the joint rotation β is given by

$$\delta = t_j \gamma = R_j \beta \tag{17}$$

R_j is the radius of the interface at the joint position, which is shown in Fig. 4. The infinitesimal force dF in the adhesive joint due to shear stresses from the bending of the pole which is acting on the joint circumference, is

$$\mathrm{d}F = \tau l R_j \cos\varphi \mathrm{d}\varphi \tag{18}$$

and since the moment arm is $R_j\cos\varphi$, the corresponding moment dM is

$$\mathrm{d}M = R_j \cos\varphi \mathrm{d}F = \tau l R_j^2 \cos^2\varphi \mathrm{d}\varphi \tag{19}$$

Introducing Eq. (18) as well as the stress-strain relation $\tau=G\gamma$ (with G being the shear modulus of the applied resin) into Eq. (19) and integrating over the circumference, gives the following equation

$$M = \left(\int_0^{2\pi} G \frac{R_j}{t_j} l R_j^2 \cos^2\varphi \mathrm{d}\varphi \right) \beta \tag{20}$$

Considering the joint as a rotational spring, the term in the parenthesis is the spring constant c_f, corresponding to the bending stiffness of the joint that is (Raftoyiannis and Polyzois 2007)

$$c_f = G \frac{\pi R_j^3}{t_j} l \tag{21}$$

Finally, the dimensionless rotational spring stiffness C_f, is introduced as follows:

$$C_f = \frac{c_f}{\frac{E_{eff} \pi R_j^3 h}{L/2}} \tag{22}$$

where the denominator in Eq. (22) corresponds to the mean bending stiffness of both segments at the joint position.

5. Precise time integration method

Neglecting the damping effect, the forced vibration equation is (Rao 1995)

$$[M]\ddot{\underline{\delta}} + [K]\underline{\delta} = \underline{Q}(t) \tag{23}$$

where [*M*] and [*K*] are the total mass and stiffness matrices, respectively and $\underline{\delta}$, is the displacement vector.

One of the highly precise methods for solving the time equations of dynamic analysis is the precise time integration method (Zhong and Williams 1994). This method cannot only give the precise numerical results, but also has an explicit integral scheme and unconditional stability. Assume the following

$$\underline{p} = [M]\dot{\underline{\delta}} \tag{24}$$

The second-order differentials in Eq. (23) can be transformed into the first-order form as

$$\dot{\underline{v}} = H\underline{v} + \underline{f} \tag{25}$$

where

$$\underline{v} = \begin{Bmatrix} \underline{q} \\ \underline{p} \end{Bmatrix}, \quad H = \begin{bmatrix} A & D \\ B & G \end{bmatrix}, \quad \underline{f} = \begin{Bmatrix} \{0\} \\ \underline{Q}(t) \end{Bmatrix}, \quad \underline{q} = \underline{\delta} \tag{26}$$

and

$$A = [0],\ B = -[K],\ G = [0],\ D = [M]^{-1} \tag{27}$$

By considering Eq. (25), it is possible to obtain its general solution

$$\underline{v} = e^{Ht}\underline{v}_0 + \int_0^t e^{H(t-\xi)}\underline{f}(\xi)d\xi \tag{28}$$

Suppose that the time step is $\lambda = t_{k+1} - t_k$, then Eq. (22) becomes

$$\underline{v}_{k+1} = T\underline{v}_k + \int_{t_k}^{t_{k+1}} e^{H(t_{k+1}-\xi)}\underline{f}(\xi)d\xi \tag{29}$$

where $T=e^{H\lambda}$.

Considering that the nonlinear term is approximately linear within a very small time step (t_k, t_{k+1}) (Tang 2008)

$$\underline{f}(t) = \underline{r}_0 + \underline{r}_1(t - t_k) \tag{30}$$

Using the straight line equation within the time step

$$\underline{f}(t) - \underline{f}(t_k) = \frac{\underline{f}(t_{k+1}) - \underline{f}(t_k)}{t_{k+1} - t_k}(t - t_k) \tag{31}$$

Thus

$$\underline{r_1} = \frac{\underline{f}(t_{k+1}) - \underline{f}(t_k)}{\tau}, \quad \underline{r_0} = \underline{f}(t_k) \tag{32}$$

Now, substituting Eq. (30) into Eq. (29) gives the precise time integration equation as follows

$$\underline{v_{k+1}} = T \times [\underline{v_k} + H^{-1}(\underline{r_0} + H^{-1}\underline{r_1})] - H^{-1}(\underline{r_0} + H^{-1}\underline{r_1} + \underline{r_1}\lambda) \tag{33}$$

6. Numerical results and discussion

In the numerical analysis presented in this study, to model the dynamic loads applied to the transmission poles, two locations on the poles are considered. One at the pole tip to model the tension force of the cables that may be applied dynamically due to the factors such as wind gusts or cable unilateral failure, and the other at about 80 cm from the pole base. The second location for the application of the load is adopted, because the transmission poles are mainly located near the streets and roads, and they are subjected to impact of the passing vehicles.

The impulse loads considered in the current study are step, triangular and sine pulses whose time functions are as follows (T_1 is the fundamental period of the pole)

Step pulse:
$$f(t) = \begin{cases} f_0 \xrightarrow{if} 0 \le t \le T_1 \\ 0 \xrightarrow{if} t > T_1 \end{cases} \tag{34}$$

Triangular pulse:
$$f(t) = \begin{cases} 2f_0(t/T_1) \xrightarrow{if} 0 \le t \le T_1/2 \\ -2f_0(t/T_1 - 1) \xrightarrow{if} T_1/2 < t \le T_1 \\ 0 \xrightarrow{if} t > T_1 \end{cases} \tag{35}$$

Sine pulse:
$$f(t) = \begin{cases} f_0 \sin(\pi.t/T_1) \xrightarrow{if} 0 \le t \le T_1 \\ 0 \xrightarrow{if} t > T_1 \end{cases} \tag{36}$$

6.1 Impulse loads at the pole tip

By combining the formulation of the tapered beam element, the flexible connection model and the precise time integration method, a computer code for the transient dynamic analysis of jointed FRP poles (neglecting the damping effect) is provided by MATLAB 7.1 software. Fig. 6 shows the algorithm of the developed FE code.

A typical jointed pole named as pole "*A*" with the geometric characteristics listed in Table 1, made from E-glass/polyester having the fiber volume fraction of 0.65 (whose material properties are available in Table 2), with $[(-10/10)_2]$ lay-up with respect to the pole axis, is considered. This pole contains a flexible joint at the half of its length whose characteristics are found in Table 3. At the first step, the pole "*A*" subjected to step, triangular and sine pulses having a maximum force of 1 kN (Fig. 5) is analyzed by the present finite element model (the fundamental period of the typical pole is 0.156 sec).

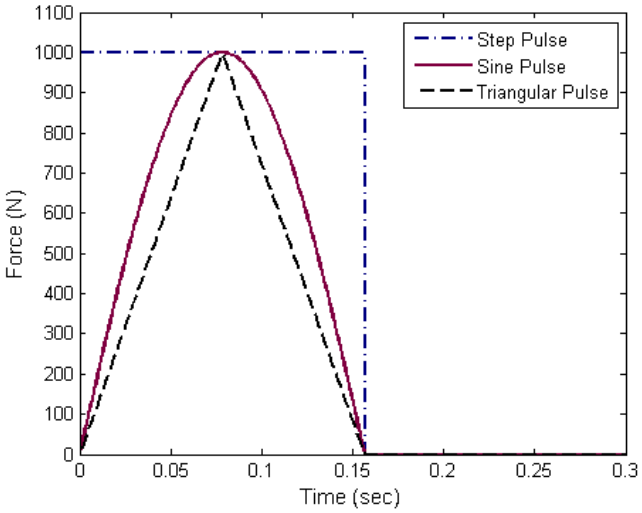

Fig. 5 Step, triangular and sine pulses applied at the tip of the typical pole "*A*"

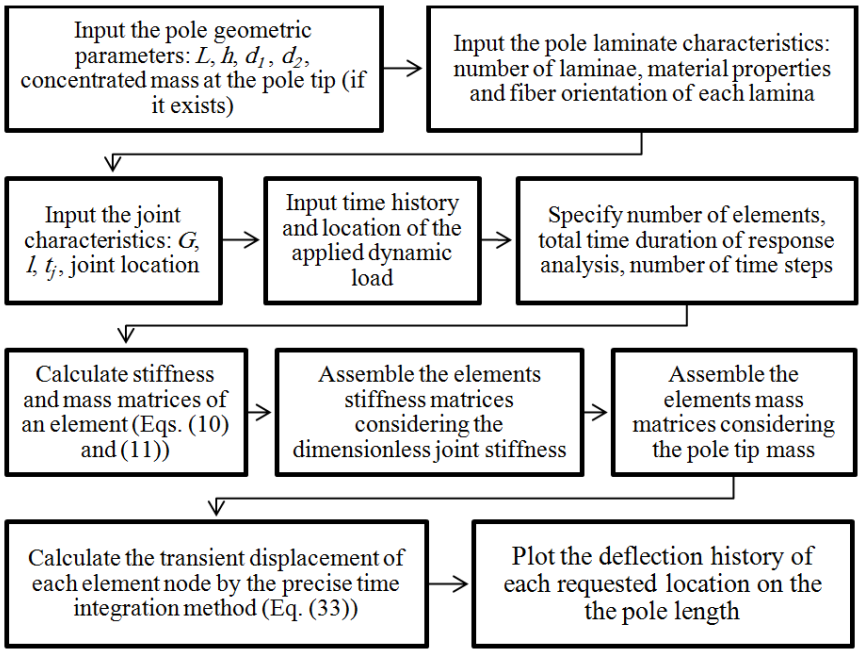

Fig. 6 The algorithm of the developed FE code using MATLAB software

Table 1 Geometric characteristics of the jointed pole "*A*"

Length of each part (mm)	Material type	Tapered angle of each part	Tip diameter of top part, d_1 (mm)	Base diameter of bottom part, d_2 (mm)	Wall thickness, t (mm)	Number of laminae
3050	E-glass/polyester (with fiber volume fraction = 0.65)	0.477˚	119	210	2.4	4

Table 2 Properties of E-glass/polyester unidirectional lamina with fiber volume fraction V_f=0.65 (Polyzois *et al*. 1998)

Longitudinal modulus, E_L (GPa)	Transverse modulus, E_T (GPa)	Shear modulus, G_{LT} (GPa)	Major Poisson's ratio, ν_{LT}	Density, ρ (kg/m^3)
48	13.30	5.17	0.235	1904

Table 3 Joint characteristics (Raftoyiannis and Polyzois 2007)

Adhesive: West System Epoxy 105 with hardener 206				Adhesive thickness, t_j (mm)	Joint length (mm)
Elasticity modulus (GPa)	Tensile strength (MPa)	Poisson's ratio	Density (kg/m^3)		
3.172	50.47	0.3	1180	0.45	305

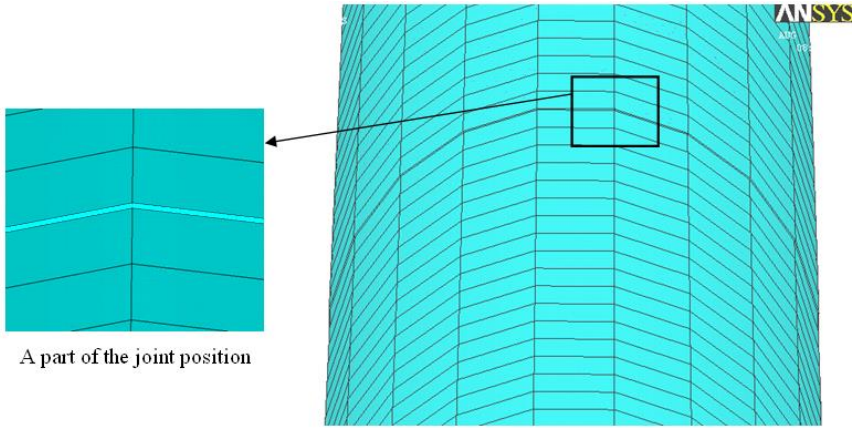

Fig. 7 Joint region of the jointed pole "*A*" for ANSYS model

In order to validate the results obtained from the present model, the jointed pole with total length of 5795 mm was also analyzed by ANSYS 11.0 commercial finite element software.

In the ANSYS model, each part of the pole is discretized by the total number of 2000 elements of the type SHELL99 and the joint adhesive region by 400 elements of the type SOLID95. Surface-to-surface contact from bonded type is defined in the software between the adhesive outer surface and the pole inner surface for the upper part, and also between the adhesive inner surface and the pole outer surface for the lower part, using CONTACT174 and TARGET170 elements (ANSYS 2007) (Fig. 7). Then, a cohesive zone material model is added to the contact elements material properties, which has only provided with the new versions of ANSYS software (version 11.0 and the newer ones). For comparison, the deflection of the pole tip (the maximum deflection) within the applied duration of each pulse, for both the tapered beam finite element and the ANSYS models, are shown in Figs. 8 to 10. Using a computer with a 3.06 GHz processor and 1.5 gigabytes of physical memory, in the case of triangular impulse loading, the run time of the ANSYS model is computed as 4422 sec (about 74 minutes), while the analysis duration of the provided code by the tapered element model is computed to be only 2 sec.

As it is observed in Figs. 8 to 10, there is an excellent agreement between the presented formulation and the ANSYS models. The maximum discrepancy within the duration of the applied

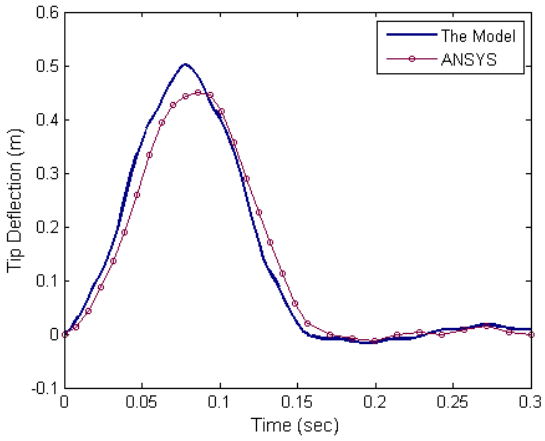

Fig. 8 Tip deflection history of the pole "*A*" with [(-10/10)$_2$] lay-up under step pulse at the pole tip

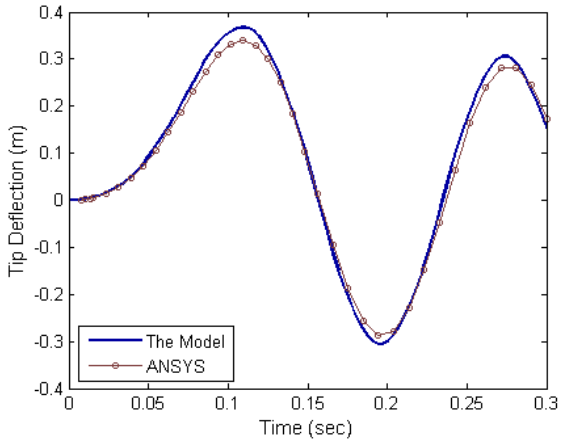

Fig. 9 Tip deflection history of the pole "*A*" with [(-10/10)$_2$] lay-up under triangular pulse at the pole tip

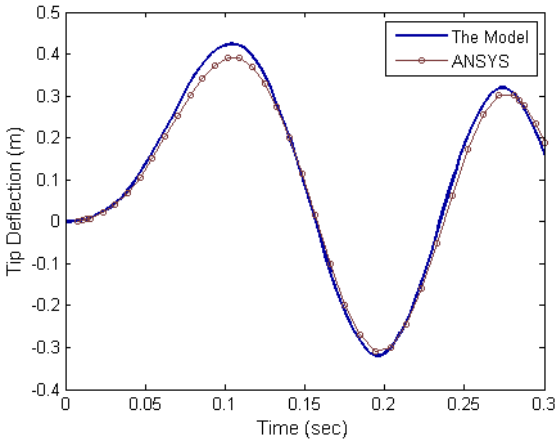

Fig. 10 Tip deflection history of the pole "*A*" with [(-10/10)$_2$] lay-up under sine pulse at the pole tip

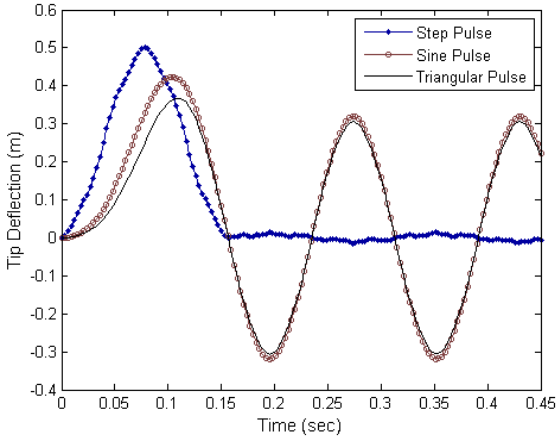

Fig. 11 Comparison of tip deflection history of the pole "*A*" with [(-10/10)$_2$] lay-up under various pulses at the pole tip

pulse occurred in the case of step pulse and it is 11%. For other cases, the discrepancy is less. The other conclusion obtained from these figures is that the maximum deflection of the pole in the case of step pulse is greater than the maximum deflection obtained in the cases of triangular and sine pulses, having the same maximum force amplitude. This is because, the area under the force-time diagram which is a measure of the impact quantity, is greater for the step pulse compared to the other two pulses (Fig. 5). In addition, the trends of the tip deflection history of the pole under the triangular and the sine pulses are similar to each other, but are different from the step pulse. The maximum deflection corresponding to the sine pulse is greater than the maximum deflection of the triangular pulse. These results are shown in Fig. 11. The maximum deflection of the pole occurred at earlier time for step pulse compared to the other pulses. It is exactly at the half time of the impulse duration.

In order to evaluate the influence of the joint stiffness on the dynamic response of the poles, the

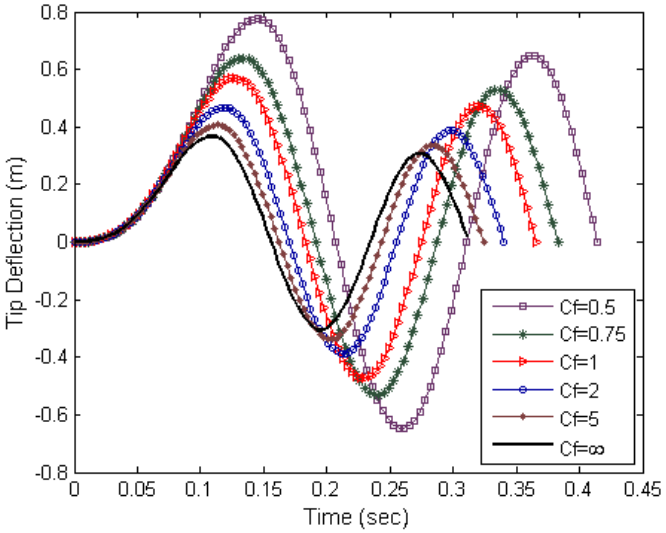

Fig. 12 Tip deflection history of the pole "*A*" with $[(-10/10)_2]$ lay-up under triangular pulse at the pole tip, for various dimensionless joint stifnesses

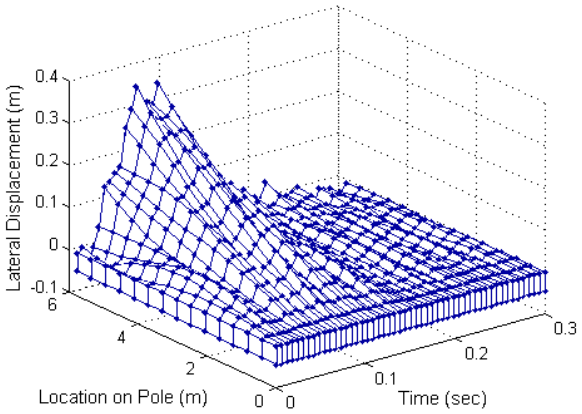

Fig. 13 Deflection history of the pole "*A*" with $[(-10/10)_2]$ lay-up under step pulse applied at the height of 80 cm from the base

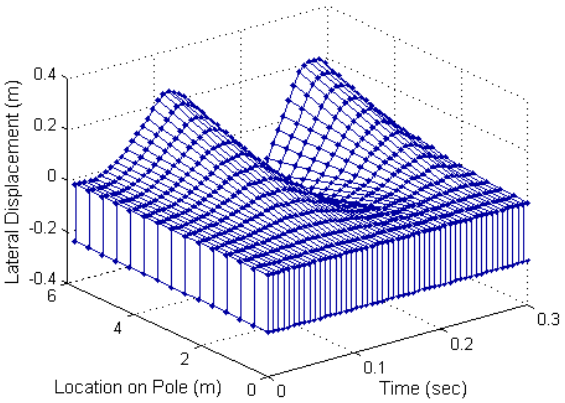

Fig. 14 Deflection history of the pole "*A*" with $[(-10/10)_2]$ lay-up under triangular pulse applied at the height of 80 cm from the base

tip deflection history of the pole "*A*" with $[(-10/10)_2]$ lay-up, under triangular pulse with the maximum load of 1 kN is illustrated for various dimensionless flexural stiffnesses of the joint in Fig. 12. It is observed that by increasing the joint stiffness, the amplitude of the pole tip deflection history decreases and the time of occurrence of the maximum deflection is earlier; as for the case $C_f = \infty$, which indicates the continuous pole, the pole tip deflection amplitude has the minimum value.

6.2 Impulse loads at the height of 80 cm from the base

To model the probable impacts imparted to the transmission poles by passing vehicles, the

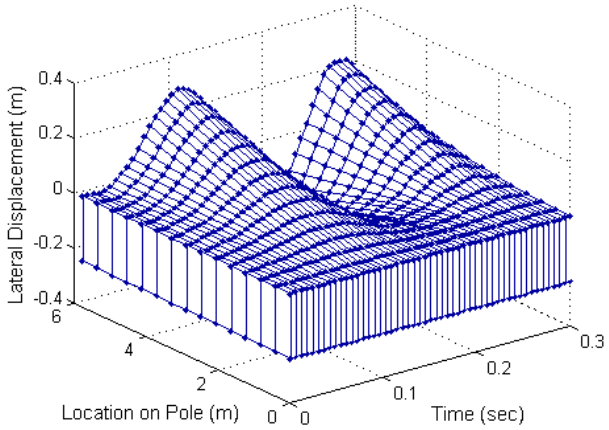

Fig. 15 Deflection history of the pole "*A*" with $[(-10/10)_2]$ lay-up under sine pulse applied at the height of 80 cm from the base

location of the application of various pulses is considered at the height of 80 cm from the base. Thus, the typical pole "*A*" with $[(-10/10)_2]$ lay-up, subjected to step, triangular and sine pulses with the maximum load of 30 kN, applied to the pole at the height of 80 cm from the base, is analyzed and the deflection histories of the entire pole are illustrated in Figs. 13, 14 and 15, respectively. Comparing these figures with Figs. 8 to 10 reveals that if the location of the applied impact load is at the distance of 80 cm from the base, a greater impulse load (30 times), can create the same maximum deflection as to apply impulse load at the pole tip. It is observed that by applying the load at the distance of 80 cm from the base, the maximum deflection occurs at the pole tip. The maximum deflection occurs for step, sine, and then triangular pulses, respectively.

It is to be noted that in the case of step pulse loading at the height of 80 cm from the pole base, at some of the time intervals, the maximum deflection occurs in a position other than the pole tip (Fig. 13). That is, applying the step pulse causes the pole to vibrate, while the second mode shape is dominant at some of the time intervals, unlike the application of the impulse load at the tip, in which the pole vibrates with the fundamental mode shape as the dominant mode shape.

7. Conclusions

For transient dynamic analysis of the jointed FRP poles, a computer code was provided using a tapered beam element, a simple model considering the pole joint as a rotational spring and precise time integration method. Thereafter, the tip deflection history of a typical FRP pole with a flexible joint at the half of its length, under step, triangular and sine pulses were obtained from both the provided FE code and ANSYS model. Comparison of the resulted transient responses represented a good agreement between them. However, the analysis duration of the tapered beam finite element model found to be significantly less than the ANSYS run time. The results of the provided FE code indicated that the maximum deflection of the pole due to the step pulse is the greatest. In addition, the maximum deflection due to the sine pulse is greater than the maximum deflection corresponding to the triangular pulse, with identical peak value of the applied load. It was also observed that the jointed poles with stiffer joints have the smaller maximum deflection amplitudes.

Moreover, it was found that the deflection amplitude of the pole tip due to the applied impulse load at the height of 80 cm from the pole base is much less compared to the amplitude of the tip deflection for an impulse load with the same peak value applied to the pole tip. In the case of applied impulse at the height of 80 cm from the base, the maximum deflection occurs at the top of the pole and it is for step pulse. Furthermore, applying the impulse load at the height of 80 cm causes the pole to vibrate in a mixed mode condition in which the second mode shape is dominant at some of the time intervals.

References

ANSYS. (2007), ANSYS User's Manual for rev. 11.0. USA: ANSYS Inc.

Bae, S.H., Cho, J.R. and Jeong, W.B. (2016), "Free and transient responses of linear complex stiffness system by Hilbert transform and convolution integral", *Smart Struct. Syst.*, **17**(5), 753-771.

Caracoglia, L. (2007), "Influence of weather conditions and eccentric aerodynamic loading on the large amplitude aeroelastic vibration of highway tubular poles", *Eng. Struct.*, **29**(12), 3550-3566.

Caracoglia, L. and Jones, N.P. (2007), "Numerical and experimental study of vibration mitigation for highway light poles", *Eng. Struct.*, **29**(5), 821-831.

Caracoglia, L. and Velazquez, A. (2008), "Experimental comparison of the dynamic performance for steel, aluminum and glass-fiber-reinforced-polymer light poles", *Eng. Struct.*, **30**(4), 1113-1123.

Fam, A., Kim, Y.J. and Son, J.K. (2010), "A numerical investigation into the response of free end tubular composite poles subjected to axial and lateral loads", *Thin Wall. Struct.*, **48**(8), 650-659.

Gould, P.L. and Basu, P.K. (1977), "Geometric stiffness matrices for the finite element analysis of rotational shells", *J. Struct. Mech.*, **5**(1), 87-105.

Han, J.S., Won, B., Park, W.S. and Ko, J.H. (2016), "Transient response analysis by model order reduction of a Mokpo-Jeju submerged floating tunnel under seismic excitations", *Struct. Eng. Mech.*, **57**(5), 921-936.

Ibrahim, S. and Polyzois, D. (1999), "Ovalization analysis of fiber-reinforced plastic poles", *Compos. Struct.*, **45**(1), 7-12.

Ibrahim, S., Polyzois, D. and Hassan, D. (2000), "Development of glass fibre-reinforced plastic poles for transmission and distribution lines", *Can. J. Civil Eng.*, **27**, 850-858.

Jones, R.M. (1999), *Mechanics of Composite Materials*, CRC Press, Washington DC.

Khalili, S. and Saboori, B. (2010), "Transient dynamic analysis of tapered FRP composite transmission poles using finite element method", *Compos. Struct.*, **92**(2), 275-283.

Khdeir, A., Reddy, J. and Frederick, D. (1989), "A study of bending, vibration and buckling of cross-ply circular cylindrical shells with various shell theories", *Int. J. Eng. Sci.*, **27**(11), 1337-1351.

Lin, Z.M. (1995), "Analysis of pole-type structures of fibre-reinforced plastics by finite element method", The University of Manitoba.

Mabie, H. and Rogers, C. (1972), "Transverse vibrations of double-tapered cantilever beams", *J. Acoust. Soc. Am.*, **51**, 1771-1774.

Mabie, H. and Rogers, C. (1974), "Transverse vibrations of double-tapered cantilever beams with end support and with end mass", *J. Acoust. Soc. Am.*, **55**, 986-989.

Metiche, S. and Masmoudi, R. (2012), "Analysis and design procedures for the flexural behavior of glass fiber-reinforced polymer composite poles", *J. Compos. Mater.*, **47**(2), 207-229.

Metiche, S., Masmoudi, R. and Abdel-Baky, H. (2009), "New design procedure for FRP composites poles", *Paper presented at the the 24th American Society of Composites (ASC)*, Delaware, USA, September.

Navaratna, D.R., Pian, T.H.H. and Wittmer, E.A. (1968), "Stability analysis of shell of revolution by the finite element method", *AIAA J.*, **6**, 355-361.

Noor, A.K., Burton, W.S. and Peters, J.M. (1991), "Assessment of computational models for multilayered

composite cylinders", *Int. J. Solid. Struct*., **27**(10), 1269-1286.
Polyzois, D., Raftoyiannis, I. and Ibrahim, S. (1998), "Finite elements method for the dynamic analysis of tapered composite poles", *Compos. Struct*., **43**(1), 25-34.
Polyzois, D.J. and Raftoyiannis, I.G. (2009), "Nonlinear shell-type to beam-type fea simplifications for composite frp poles", *Arch. Appl. Mech*., **79**(4), 347-358.
Raftoyiannis, I.G. and Polyzois, D.J. (2007), "The effect of semi-rigid connections on the dynamic behavior of tapered composite GFRP poles", *Compos. Struct*., **81**(1), 70-79.
Rao, S.S. (1995), *Mechanical Vibrations*, Addison-Wesley Reading, MA.
Saboori, B. and Khalili, S. (2011), "Static analysis of tapered FRP transmission poles using finite element method", *Finite Elem. Analy. Des*., **47**(3), 247-255.
Tang, B. (2008), "Combined dynamic stiffness matrix and precise time integration method for transient forced vibration response analysis of beams", *J. Sound Vib*., **309**(3), 868-876.
Xiang, S., Bi, Z.Y., Jiang, S.X., Jin, Y.X. and Yang, M.S. (2011), "Thin plate spline radial basis function for the free vibration analysis of laminated composite shells", *MA*, **93**(2), 611-615.
Zabihollah, A. and Ganesan, R. (2010), "Buckling analysis of tapered composite beams using a higher order finite element formulation", *J. Reinf. Plast. Compos*., **29**(17), 2663-2683.
Zhong, W. and Williams, F. (1994), "A precise time step integration method", *Proceedings of the Institution of Mechanical Engineers, Part C: Journal of Mechanical Engineering Science*, **208**(6), 427-430.

CC